Cold Regions Science and Technology 208 (2023) 103794

Contents lists available at ScienceDirect

Cold Regions Science and Technology

journal homepage: www.elsevier.com/locate/coldregions

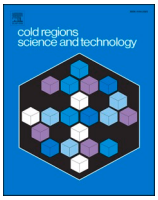

Tracking changes in the fjord environment over a winter season using ice bulk salinity and $\delta^{18}O$

Megan O'Sadnick [a,b,*], Chris Petrich [b], Jofrid Skarðhamar [c]

[a] Department of Physics and Technology, UiT The Arctic University of Norway, Tromsø 9019, Norway
[b] SINTEF Narvik, Narvik 8517, Norway
[c] Institute of Marine Research, Tromsø 9007, Norway

ARTICLE INFO

Keywords:
Fjord ice
Ice-ocean interface
Ice growth rate
Bulk ice properties
River-ocean interaction

ABSTRACT

Ice that forms in the fjords of northern Norway often undergoes temperature fluctuations, rising above and below freezing, throughout winter and experiences variable conditions at the ice-ocean interface due to changes in freshwater runoff from surrounding land. Conditions at the interface can be difficult to track throughout the season without consistent measurement, resultantly limiting understanding of how freshwater runoff from land may impact a fjord throughout winter. Ice samples gathered from fjords, however, offer a unique opportunity to examine the connection between bulk ice properties like salinity and $\delta^{18}O$ and environmental conditions including growth rate and the composition of water at the interface. Using relationships from the literature, a method was developed to invert bulk ice salinity and $\delta^{18}O$ simultaneously to determine the history of growth rate and interface water composition of ice samples gathered in March 2018 from six fjords located in northern Norway. Quantitative results depend on knowledge of salinity and $\delta^{18}O$ of both the seawater and freshwater leading into the fjord. It was found that five of the six investigated sites had ice grown from a brackish layer with 0 to 40% seawater content, while one site had ice grown from water with 50 to 90% seawater content. The brine volume fraction of the ice from four out of the six fjords was partly or entirely below 5% which is too low to allow for efficient brine transport. It is additionally shown that at ice temperatures between −2 and 0 °C, ice grown from water having a composition of up to 30% seawater at the ice ocean interface will fall below the 5% brine volume fraction, depending on growth rate. Through use of this method, an improved understanding was obtained of fluctuations in the composition of water at the ice-ocean interface in a sub-arctic coastal environment and, when ice growth rate is considered, the substantial influence on ice bulk properties.

1. Introduction

Norwegian fjords act as a natural laboratory to observe the interaction of fresh water, fed by snow melt, rain, and ground water with the ocean from periods of relative warmth through winters with sub-freezing temperatures. Fjord circulation is controlled by water exchange with coastal waters, tides, river runoff, local and regional winds combined with the bathymetry and shape of the fjord (Asplin et al., 1999, Aure et al., 1996, Inall and Gillibrand, 2010; Stigebrandt, 2012). Fjords are often surrounded by high mountains with no two fjords exactly alike in their weather including air temperature, precipitation, and wind patterns (Cottier et al., 2010). The ice that can develop on the surface is likewise variable, a reflection of the environmental conditions at the time of its formation. In Norway, 47 fjords and coastal areas of 386 examined were found to have >5 km^2 of ice between 2001 and 2019 (O'Sadnick et al., 2020). The ice that forms in the sub-arctic fjords of Norway can be composed largely or entirely of snow ice, and greatly influenced by the freshwater draining into the fjord during the winter (Green et al., 2004; Skreslet and Loeng, 1977). These characteristics are not consistent however and generalizations about ice properties in Norwegian fjords are problematic. With increasing warming in the arctic, the physical processes observed in fjords including the influence of freshwater at the ice-ocean interface, its incorporation into ice and potential impact on other properties such as microstructure are an important area of focus (Alkire et al., 2015; Kujawa et al., 2021). Coastal regions are diverse in their ecology (Vonnahme, 2020; Wassmann et al., 1996) and also heavily traversed by humans (Olsen et al., 2019; Svavarsson et al., 2021). Understanding how and why ice may form and its

* Corresponding author.
E-mail address: megan.osadnick@sintef.no (M. O'Sadnick).

https://doi.org/10.1016/j.coldregions.2023.103794
Received 28 September 2022; Received in revised form 16 December 2022; Accepted 31 January 2023
Available online 11 February 2023

properties are imperative to the future environmental management of these regions.

To obtain a description of growth conditions and enhance understanding of why ice differs from fjord to fjord and between years, ice bulk salinity and oxygen isotope composition, $\delta^{18}O$, are two characteristics of ice that are helpful to measure. The latter, the ratio of ^{18}O to ^{16}O, is the isotopic signature of the ice and defined as:

$$\delta^{18}O = \left[\frac{\left(\frac{^{18}O}{^{16}O}\right)_s}{\left(\frac{^{18}O}{^{16}O}\right)_{VSMOW}} - 1 \right] * 1000‰ \quad (1)$$

where subscript *s* represents the ratio of the sample and *VSMOW* refers to Vienna Standard Mean Ocean Water. $\delta^{18}O$ can differ between samples having equal values for salinity due to its link to the origin of fresh water that mixes with seawater at the ice-ocean interface. The isotopic signature of fresh river water varies considerably across the globe having an average $\delta^{18}O$ value of −10.59 ‰ (Nan et al., 2019) with variation due to the composition of precipitation and degree of evaporation. In Norway specifically, $\delta^{18}O$ can range between approximately −4 ‰ in southern Norway and approximately −12 ‰ in northern Norway (Nan et al., 2019). The isotopic signature of ocean water is also not a constant. While Vienna Standard mean ocean water has a $\delta^{18}O$ of 0 ‰ by definition, values as high as approximately 2 ‰ at lower latitudes to as low as approximately −3 ‰ in regions of the arctic have been measured (LeGrande and Schmidt, 2006).

As ice forms, ^{18}O is preferentially incorporated into the ice due to its lower vibrational energy in comparison to ^{16}O (Eicken, 1998) (Fig. 1). The difference between $\delta^{18}O$ in the seawater and ice is termed the effective fractionation coefficient (ε_{eff}):

$$\varepsilon_{eff} = \delta^{18}O_{ice} - \delta^{18}O_{water} \quad (2)$$

Under isotopic equilibrium, whereby ice is grown in a laboratory at a rate slow enough to allow for mixing of the boundary layer, ε_{eff} is estimated to be 2.91 ‰ for pure freshwater ice (Lehmann and Siegenthaler, 1991). For sea ice, under laboratory conditions at the slowest of growth rates, fractionation was measured to be 2.7 ‰ (Craig and Hom, 1968). Many examples of measurements of natural sea ice of differing growth rate exist in the literature, with ε_{eff} values of, for example, 2.09 ‰ (Melling and Moore, 1995), 2.57 ‰ (Macdonald et al., 1995), 2.23 ‰ (Macdonald et al., 1999), and 1.88 ‰ (Toyota et al., 2013).

A boundary layer is defined as the water adjacent to the ice interface where transport occurs through diffusion only. The thickness of the boundary layer at the ice-ocean interface depends in part on the rate of ice growth which will affect the convection ahead of the freezing front due to salt rejection and diffusion of, in this application, $H_2^{18}O$. For a constant growth rate, the thicker the boundary layer the lesser the amount of effective fractionation that will occur as seawater freezes to sea ice. This, in turn, will lead to lowering values of $\delta^{18}O$ in the ice. Burton et al. (1953) derived the original stagnant boundary model used in subsequent work examining the link between growth rate and fractionation. Weeks and Lofgren (1967) found this work described well the segregation of salt during the freezing of sea water, deriving boundary layer thickness in lab- based experiments which were later used in studies of Arctic sea ice. Souchez and Tison (1987, 1988) next examined the fractionation of deuterium during the growth of sea and freshwater ice and the impact of growth rate. Eicken (1998) further built upon this work to derive an empirical relationship between effective fractionation, ε_{eff}, and growth rate by assuming constant values for diffusion, boundary layer thickness, and an equilibrium fractionation factor that describes the isotopic ratios in the solid and liquid phases. Smith et al. (2012) showed that this model often underestimates values of growth rate in sea ice based on field data obtained in Antarctica. Laboratory and observational data from another study focused on the Sea of Okhotsk and the Antarctic seas further support this finding (Toyota et al., 2013). In the latter, the authors worked to improve the fit of the Eicken (1998) model to data gathered on laboratory- grown and natural sea ice, using a least-squares fitting procedure to determine values for boundary layer thickness and the effective fractionation coefficient. While it was necessary to apply two procedures, fitting separately to lab and field measurements, Toyota et al. (2013) derived a single formula for the effective fractionation coefficient for sea ice ($\varepsilon_{eff,si}$) to cover growth rates of 0.8×10^{-7} m s^{-1} to 9.3×10^{-7} m s^{-1}.

Both bulk salinity and $\delta^{18}O$ depend on conditions at the ice-ocean interface and growth rate, albeit in different ways. In the regions considered here and based on previous work, a greater fraction of fresh water will both reduce $\delta^{18}O$, and salinity at the interface and in the ice. Growth rate, however, has an opposite impact on bulk ice salinity. A faster growth rate leads to less time for salt to be rejected from the ice as it is forming leading to higher bulk salinity while $\delta^{18}O$ will have a lower value due to a lesser amount of fractionation (see Eqs. 1 and 2) (Eicken, 1998; Petrich et al., 2011).

Exploration of the relationship between bulk ice salinity, source water, and growth rate had initially focused on the initial rejection of salt during formation with studies presenting relationships between growth velocity and a segregation coefficient (e.g. Weeks and Lofgren, 1967; Cox and Weeks, 1975; Nakawo and Sinha, 1981). The latter is

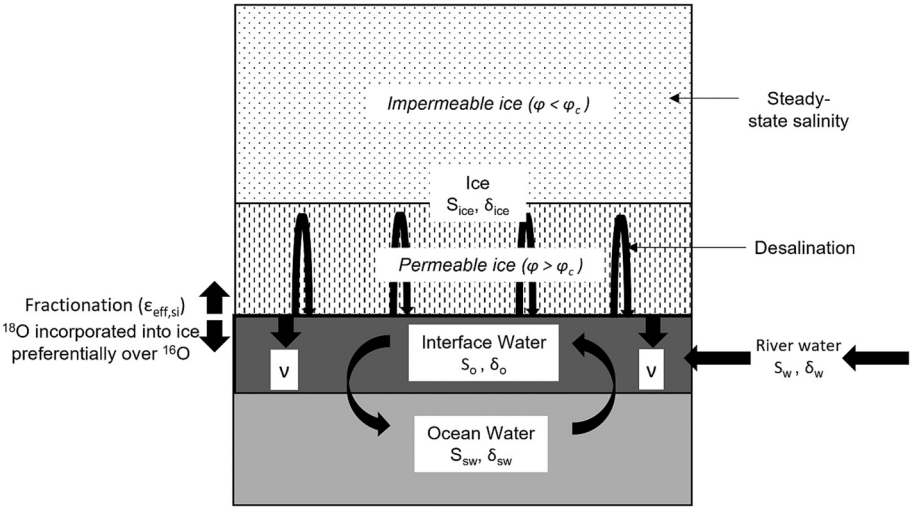

Fig. 1. Schematic of ice volume as ice growth occurs and ocean and river water mixes at the ice ocean interface. Adapted from Petrich et al. (2011).

used to quantify the ratio of salt in the ice to that in the water at the ice-ocean interface after Burton et al. (1953) for seawater salinities >30 psu. Granskog et al. (2006) focused on Baltic sea ice forming from seawater having a mean salinity of 3.2 psu. It was found that previous models overestimate the segregation coefficient in application to low-salinity water and ice. In more recent works examining the formation of sea ice and the desalination processes, greater focus is placed on gravity drainage of brine often applying concepts described by mushy layer theory (Hunke et al., 2011; Notz and Worster, 2009; Worster, 1997). In line with these more recent studies, Petrich et al. (2011) sought an explicit expression for bulk salinity segregation of a steadily growing layer of ice. Desalination was based on gravity drainage and assumed to be confined to ice of a brine volume fraction above a pre-defined characteristic brine volume fraction, φ_C (Fig. 1). Desalination rates were calibrated against results of a computational fluid dynamics model.

In the following study, the relationships presented by Toyota et al. (2013) and Petrich et al. (2011) were applied using measurements of ice bulk salinity and $\delta^{18}O$, river $\delta^{18}O$, and seawater $\delta^{18}O$ and salinity to determine the properties of water at the interface and the growth rate at six fjords located in northern Norway (Fig. 2). The connection to weather and oceanographic patterns in each fjord and how this may be tied to ice properties within the ice is also discussed.

2. Methods

2.1. Derivation of growth rate and fraction of seawater from ice properties

In this study, the fraction of seawater in comparison to freshwater, F_{sw}, and ice growth rate, ν, were determined from measurements of ice bulk salinity (S_{ice}) and $\delta^{18}O$ (δ_{ice}) and seawater and freshwater properties. As displayed in Fig. 1, water at the ice-ocean interface is assumed to be a mixture of seawater and freshwater with values for salinity and $\delta^{18}O$ (S_o, δ_o) determined from:

$$S_0 = F_{sw}S_{sw} + (1 - F_{sw})S_w, \tag{3}$$

$$\delta_o = F_{sw}\delta_{sw} + (1 - F_{sw})\delta_w, \tag{4}$$

Where F_{sw} is the fraction of seawater in comparison to freshwater ($F_w = 1 - F_{sw}$), S_{sw} and S_w are the salinity of the seawater and freshwater in practical salinity units (psu), respectively, and δ_{sw} and δ_w are $\delta^{18}O$ for

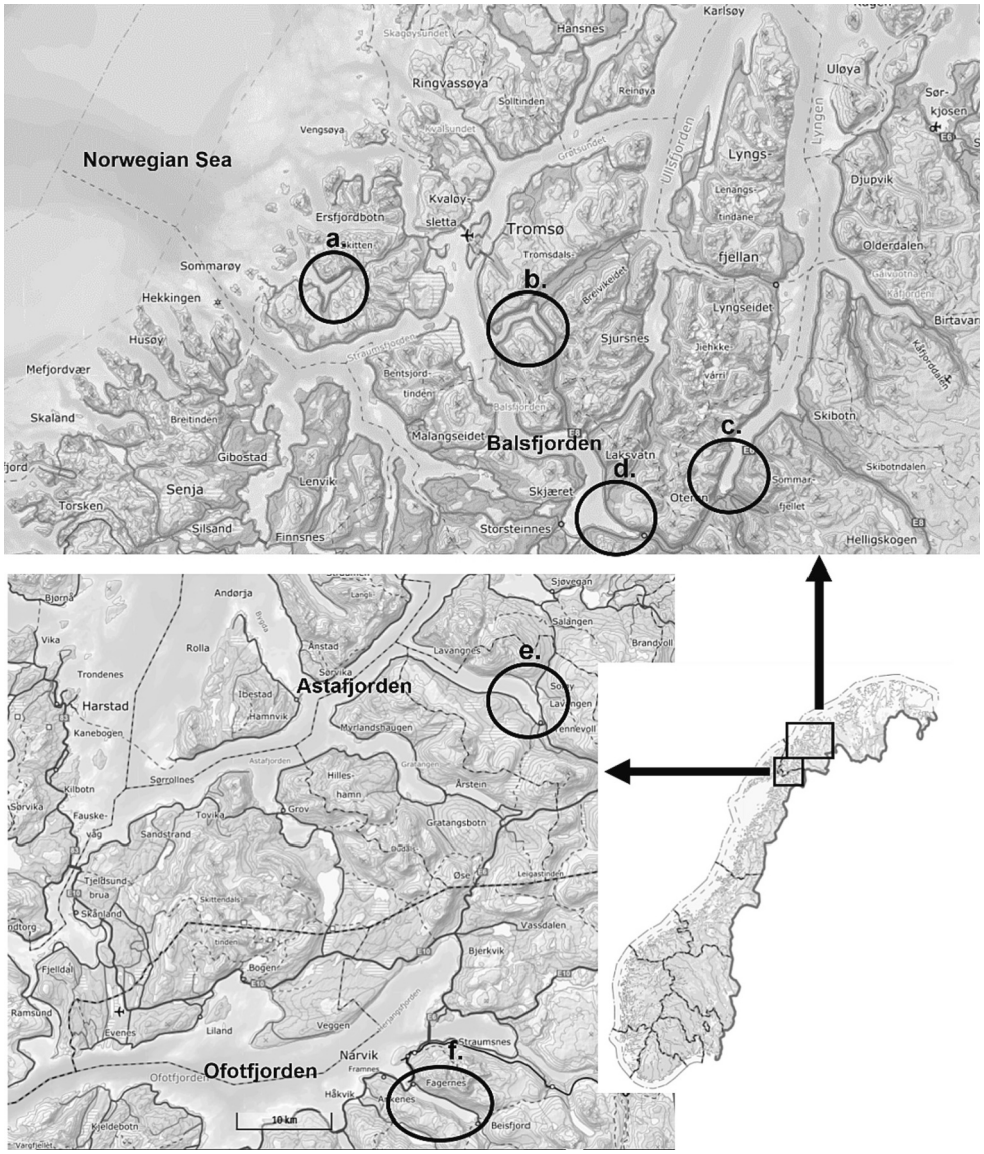

Fig. 2. Location of six fjords in northern Norway where ice core samples were gathered. a) Kattfjord (sample gathered at 69° 37.928′ N, 18° 22.930′ E); b) Ramfjord (sample gathered at 69° 31.491′ N, 19° 13.607′ E); c) Storfjord (sample gathered at 69° 17.064′ N, 19° 56.735′ E); d) Nordkjosbotn (sample gathered at 69° 13.354′ N, 19° 30.059′ E); e) Lavangen (sample gathered at 68° 45.345′ N, 17° 47.408′ E); and f) Beisfjord (sample gathered at 68° 22.824′ N, 17° 35.293′ E). ©Kartverket.

seawater and freshwater in parts per thousand (‰). Seawater properties, S_{sw} and δ_{sw}, were measured during each field visit, and δ_w was measured at the main river flowing into each fjord the following season (Tables 2 & 3). Salinity of freshwater was not measured and is assumed to be $S_w = 0$. Eq. 3 therefore simplifies to:

$$S_0 = F_{sw} S_{sw}, \tag{5}$$

Seawater properties refer here to values measured >1 m below the ice-ocean interface.

Toyota et al. (2013) linked the effective fractionation coefficient of sea ice ($\varepsilon_{eff,si}$) to ice growth rate, ν, using:

$$\varepsilon_{eff,si} = a_1 + b_1 exp\left(-\frac{\nu}{c_1}\right) + d_1 exp\left(-\frac{\nu}{e_1}\right), \tag{6}$$

Where $a_1 = 1.2280$ ‰, $b_1 = 0.7311$ ‰, $c_1 = 8.0100 \bullet 10^{-8}$ m s^{-1}, $d_1 = 0.8441$ ‰, $e_1 = 0.7800 \bullet 10^{-6}$ m s^{-1} being valid for $0.8 \bullet 10^{-7}$ m s^{-1} < ν < $9.3 \bullet 10^{-7}$ m s^{-1}.

A definition for δ_{ice} can therefore be formulated combining Eq. (2), Eq. (4), and Eq. (6) that is dependent on two unknowns, F_{sw} and ν:

$$\delta_{ice} = F_{sw}\delta_{sw} + (1 - F_{sw})\delta_w + a_1 + b_1 exp\left(-\frac{\nu}{c_1}\right) + d_1 exp\left(-\frac{\nu}{e_1}\right), \tag{7}$$

Petrich et al. (2011) linked the bulk salinity of sea ice, S_{ice}, to the interface salinity, S_0, and ice growth rate, ν. S_0 depends on F_{sw} according to Eq. (5), and can be related to S_{ice} through the expression presented by Petrich et al. (2011):

$$\frac{S_{ice}}{S_0} \approx \frac{\rho_o}{\rho_{ice}} \frac{C\,\varphi}{C_0}, \tag{8}$$

Where S_{ice}, ρ_{ice}, and C are the salinity, density, and brine concentration in the ice, respectively, S_0, ρ_0, and C_0 are salinity, density, and solute concentration of seawater at the ice-ocean interface, respectively, and ϕ is brine volume fraction. At the point in the ice where the brine volume fraction falls below a characteristic brine volume fraction (ϕ_c), defined as the approximate brine volume fraction ice transitions from permeable with movement of brine through pore space to impermeable with steady- state salinity to the following expression is found as a function of growth velocity, ν (Petrich et al., 2011):

$$\frac{(C\varphi)_c}{C_0} = \varphi_C \left(1 + \left(\frac{\varphi_c}{2}\frac{\nu}{\gamma_s w_0}\left[-1 + \sqrt{1 + \frac{4(1-\varphi_c)}{\varphi_c^2}\frac{\gamma_s w_0}{\nu}}\right]\right)\right), \tag{9}$$

Where:

$$\gamma_s w_0 = \frac{4.5\ x\ 10^{-8}\frac{m}{s}}{34\ \frac{kg}{m^3}} C_0, \tag{10}$$

$$C_0 = \frac{\rho_o\left(\frac{S_0}{1000}\right)}{\left(1 - \frac{S_0}{1000}\beta\right)}, \tag{11}$$

With $\gamma_s \omega_0$ being the vertical flux within the permeable zone (Golden et al., 1998), $\phi_c = 0.05$, $\beta = 0.8$ (representative of the dependence of brine density on salinity), $\rho_0 = 1026$ kg m^{-3}, $\rho_{ice} = 917$ kg m^{-3}. Through substitution of Eq. (5) and Eq. (9) into Eq. (8), a definition for S_{ice} dependent on the same two unknowns as Eq. (7), ν and F_{sw}, is provided:

$$S_{ice} = F_{sw} S_{sw} \left(\frac{\rho_o}{\rho_{ice}}\right) \varphi_C \left(1 + \left(\frac{\varphi_c}{2}\frac{\nu}{\gamma_s w_0}\left[-1 + \sqrt{1 + \frac{4(1-\varphi_c)}{\varphi_c^2}\frac{\gamma_s w_0}{\nu}}\right]\right)\right) \tag{12}$$

To determine ν and F_{sw} for each section of core having a measurement of δ_{ice} and S_{ice}, Eq. (7) and Eq. (12) are solved simultaneously through residual minimization. Thus, what is referred to as a model in the following is an inversion of equations presented by Toyota et al. (2013) and Petrich et al. (2011).

2.2. Field measurement of ice bulk properties and water endmembers

Six fjords located in northern Norway, shown in Fig. 2, were chosen for collection of ice samples in March 2018. For all fjords, this visit coincided with the end of a period where air temperatures were consistently below 0 °C, little if any snowfall occurred, and ice was presumably undergoing growth. While sampling continued in 2019 and 2020, data from the 2018 was chosen due to the minimal snowfall and a sustained period of air temperature below 0 °C (Fig. 6). On the day of sample collection, air temperatures were above −5 °C for all fjords with new snow present and little, if any, further ice growth. For a complete description of the fjords including bathymetry and geometry see O'Sadnick et al. (2022). In each fjord, at least one ice core was collected near to the center of the ice cover and between 0.5 and 1.5 km from the outlet of the main river. After measuring the depth of any snow cover, snow was removed and ice cores drilled. Upon removal, cores were quickly laid horizontal before being sliced into 0.05 m sections with each placed into a plastic bag. The ice samples were stored at room temperature to melt before measuring bulk salinity (S_{ice}) using a YSI Pro30 temperature/conductivity probe with an accuracy of 0.1 psu and resolution of ±0.1 (psu) or ± 1% of the reading. After measurement, the melted ice sample was poured into glass bottles, closed with cone-lined caps and stored at +4 °C until transport to the Stable Isotope Laboratory at the Centre for Arctic Gas Hydrate, Environment and Climate (CAGE) located at UiT The Arctic University of Norway, Tromsø, Norway where $\delta^{18}O$ analysis was performed. Measurement error was <0.01 ‰ as determined through comparison of true versus measured values of three inhouse standards of $\delta^{18}O$. Details of the analysis are given in O'Sadnick et al. (2022). A second core was drilled to measure ice temperature using a Fluke 54 II B Thermometer with a resolution of 0.1 °C and accuracy of ± [0.05% + 0.3 °C]. A zero-point test was performed showing a 0.5 °C offset, thus this is subtracted from each measurement. A third core was also gathered at each fjord for thick sectioning and analysis of ice stratigraphy. It was placed in a cooler immediately after sampling and stored in a − 18 °C freezer until it could be processed.

Also collected at each sampling site were measurements of seawater salinity, temperature, and $\delta^{18}O$ under the ice. The first two were gathered using a CTD (CastAway-CTD, Sontek) lowered manually. The temperature measurement obtained had a resolution of 0.01 °C and accuracy of 0.05 °C while the salinity measurement had a resolution of 0.01 (psu) and accuracy of ±0.1 (psu). The latter measurement provides an endmember of seawater salinity (S_{sw}). To gather a measurement of $\delta^{18}O$ of seawater (δ_{sw}), a manual water pump was lowered to between 1.5 and 2 m below the ice-ocean interface. The sample was stored in the same type of glass bottle as above for eventual measurement with the melted ice samples. Fresh water samples for measurement of $\delta^{18}O$ (δ_w) were gathered in the rivers flowing into the fjords at varying distances from the fjords. The glass bottle was similarly filled and delivered with the other samples for stable isotope analysis.

Error estimates due to uncertainty in endmember composition were performed based on a three-year record of river and seawater measurements at Beisfjord (O'Sadnick et al., 2022). While only measurements of S_{sw} δ_{sw}, and δ_w from one season are examined here, in Beisfjord additional measurements of each were made in 2018, as well as in 2019 and 2020. The standard deviations of S_{sw}, δ_{sw}, and δ_w were 0.3 psu, 0.3‰, and 0.4 ‰, respectively. For each fjord, these standard deviations are used to estimate the range of each endmember, and the model is solved to provide the uncertainty in the fraction of fresh water, growth rate, and relatedly the estimated age of the ice.

Estimations of brine volume fraction are also provided for all cores derived using measurements of bulk ice salinity and temperature. To calculate, equations and constants from Cox and Weeks (1983) meant for ice having a temperature < −2 °C and Leppäranta and Manninen (1988) for ice between −2 °C and 0 °C were applied. Air volume content was assumed to be negligible given <1 cm or negative freeboard at all sampling locations.

2.3. Ancillary data

While ice formation and breakup can occur several times during a winter season, here freeze-up is defined as the first day of consistent ice coverage with no further breakups occurring until the day of measurement. To determine the date of freeze-up, SENTINEL-1C-band Synthetic aperture radar (SAR) imagery from the vertical transmit/vertical receive (VV) polarization channel were used (Copernicus Sentintel Data, 2019) in combination with the Terra satellite MODIS MOD09A1.006 Terra Surface Reflectance 8-Day Global 500 m product. The latter does not gather imagery during the period of no sunlight in the upper latitudes (2 November – 2 February) however with correct processing steps (see O'Sadnick et al. (2020)), ice is relatively straight forward to identify. SAR imagery is available year-round but can be more difficult to interpret. While imagery is not gathered every day, a relatively narrow range for the freeze-up date can be determined. Dates of ice formation and measurement were also presented by O'Sadnick et al. (2022) and are shown in Table 1.

Values for average daily temperature and snow water equivalent, spatially interpolated onto a 1 km grid, were provided by the Norwegian Meteorological Institute and accessed using seNorge.no (Lussana et al., 2018). At each fjord, one pixel was selected at the head of each fjord located at sea level to provide local temperature. Fjord water surface temperature were derived using output from a hydrodynamic model from Institute of Marine Research (Dalsøren et al., 2020) at positions representative for the study areas.

3. Results

3.1. Initial conditions

Thin layers of ice are commonly observed in fjords throughout winter but often break up and disperse quickly. Care was therefore taken to specifically determine the freeze-up date of the ice analyzed here. Nordkjosbotn had the earliest date of continuous ice cover with freeze up occurring on 29 December 2017 followed by Kattfjord on 5 January 2018. In the other four fjords, formation occurred over a span of several weeks starting with Ramfjord on 28 January, Beisfjord on 2 February, Storfjord on 15 February, and lastly Lavangen on 27 February (Table 1).

Seawater salinities (S_{sw}), measured on the same day as ice cores were collected (Table 2), do not show large variation between fjords ranging from 32.4 psu in both Beisfjord and Nordkjosbotn to 33.4 psu in Lavangen. Similarly, $\delta^{18}O$ of seawater (δ_{sw}) only varies slightly from −0.81 ‰ at Ramfjord to −0.12 ‰ at both Lavangen and Kattfjord. Salinity is assumed to be 0 psu in all rivers (S_w). Measurements of δ_w were only gathered in Beisfjord in March 2018 with all other measurements coming the following ice season in March 2019. These values range from −12.57 ‰ to −10.24 ‰. Subsequent measurement of δ_w in 2020 and 2021 revealed little variation for each river (O'Sadnick, 2022), supporting the use of 2019 measurements despite not being collected nearer to the date of ice sampling.

3.2. Bulk ice property measurements

The cores gathered displayed a broad range of both ice bulk salinity (S_{ice}) and $\delta^{18}O$ (δ_{ice}) values (Table 3, Figs. 3)(O'Sadnick et al., 2022). Thickness ranged from 36 cm in Storfjord to 76 cm in Nordkjosbotn. Between fjords, the lowest average ice bulk salinity (S_{ice}) was found in Kattfjord with a value of only 0.3 psu ranging up to 3.9 psu in Storfjord. The lowest average ice bulk $\delta^{18}O$ (δ_{ice}) was found in Beisfjord, −8.27 ‰, while Storfjord had the highest average value, −1.42 ‰.

Ice temperature measurements showed generally a linear increase from the ice surface to the ice-ocean interface in four cores- Beisfjord, Nordkjosbotn, Storfjord, and Ramfjord. The coldest ice was found in Nordkjosbotn ranging between −4.4 up to −1.4 °C on the day of measurement. On the day of measurement, cores gathered from Lavangen and Kattfjord both were more homogeneous in temperature with all sections being above −1 °C. Despite being so warm in temperature, Kattfjord had a brine volume fraction of <5% throughout while Lavangen was entirely greater than this value. The importance of the 5% threshold is discussed further in Section 4.1. The Storfjord core also had brine volume fraction above 5% while all others were generally below this mark but not consistently, increasing and decreasing along the depth of the core.

The cores were primarily composed of congelation ice with granular ice only appearing in the upper 10 cm of the ice core in Kattfjord, 5 cm of the ice core in Beisfjord, and 1 cm in Storfjord and Ramfjord cores (Fig. 3). Ice type was determined through examination of thick sections viewed through polarized filters to determine crystal structure with images (O'Sadnick et al., 2022). In Beisfjord, this granular ice, presumably snow ice, does not show a clear $\delta^{18}O$ signature differentiating it from the congelation ice below (Fig. 4a). In Kattfjord, the upper 10 cm of the core do show minimum values of $\delta^{18}O$, presumably due to the influence of snow (Fig. 4b). Cores did display characteristics of saline ice having examples of thin elongated pores with an occasional longer channel (particularly in the Nordkjosbotn core). No evidence of a skeletal layer was observed in any cores collected.

Within one core, measurements of S_{ice} were at times relatively consistent, ranging approximately ±0.5 psu throughout the core as was the case at Lavangen (Fig. 4b) and Kattfjord (Fig. 4f). Other fjords, for example Storfjord (Fig. 4d) and Ramfjord (Fig. 4e), showed a greater range, with a difference of up to 2 psu between minimum and maximum bulk salinities of core sections. δ_{ice} measurements often showed variability between core sections where little change was recorded in salinity. For example, in ice gathered in Kattfjord (Fig. 4f), salinity hardly increased 0.2 psu in the top 25 cm, δ_{ice} seemingly shows finer detail with a range of 2.0‰ over the same depth.

3.3. Growth rate and boundary conditions at the interface

The results of the model (Eqs. 7–12), the growth rate of the ice (ν) and the fraction of seawater at the interface (F_{sw}), a proxy for the mixing occurring at the interface, are presented in Fig. 4. For all but one fjord, Storfjord, the fraction of seawater at the interface remains below 0.4 throughout the entirety of the core. This equates to ocean water at the interface not being higher than 13 psu while ice was forming. For Storfjord, the amount of seawater fluctuated from approximately 0.5 to 0.9, equivalent to between 15 and 30 psu water at the ice-ocean interface.

While fjords generally maintained air temperatures below 0 °C during ice formation, all but one experienced 1–7 days where temperatures increased slightly above 0 °C with the highest daily average temperature of 4 °C during this period recorded at Kattfjord (Table 2, Fig. 6). Kattfjord also had the highest average temperature of −5 °C. The lowest average and individual daily air temperature occurred at Storfjord, with −10 °C and − 17 °C, respectively. Snowfall, estimated as snow water equivalent (SWE) is also presented. All fjords experienced relatively little snowfall, only experiencing a few days with 1–5 mm SWE accumulation between mid-January and mid-March. This provided ice with a period of both low air temperature and little insulation on the top surface thus allowing for continuous growth except for the few days

Table 1
Summary of ice formation and measurement dates.

Fjord	Date of ice formation, 2018	Date of measurement, 2018
Beisfjord	1–5 Feb	13 Mar
Lavangen	27–28 Feb	23 Mar
Nordkjosbotn	29–30 Dec 2017	20 Mar
Storfjord	15–20 Feb	20 Mar
Ramfjord	28–29 Jan	20 Mar
Kattfjord	5–10 Jan	21 Mar

Table 2
Summary of measured endmember values for seawater (S_{sw} and δ_{sw}) and freshwater (δ_w), date of measurement for seawater and freshwater samples, and depth of measurement of the seawater sample. $S_w = 0$ psu for all cases.

Fjord	Date of Measurement	Depth from ice/ocean interface [m]	S_{sw} [psu]	δ_{sw} [‰]	Date of Measurement	δ_w[‰]
Beisfjord	19 Apr 2018	0.4	32.4	−0.34	19 Apr 2018	−12.57
Lavangen	23 Mar 2018	1.0	33.4	−0.12	14 Mar 2019	−11.34
Nordkjosbotn	13 Mar 2019	1.5	32.4	−0.17	13 Mar 2019	−12.15
Storfjord	20 Mar 2018	1.5	32.9	−0.22	12 Mar 2019	−11.55
Ramfjord	20 Mar 2018	1.5	32.5	−0.81	12 Mar 2019	−11.5
Kattfjord	21 Mar 2018	1.5	32.8	−0.12	14 Mar 2019	−10.24

Table 3
Summary of bulk ice salinities, S_{ice}, and $\delta^{18}O$, δ_{ice}, values.

Fjord	Thickness [cm]	S_{min} [psu]	S_{max} [psu]	S_{avg} [psu]	δ_{min} [‰]	δ_{max} [‰]	δ_{avg} [‰]
Beisfjord	48	0.2	1.7	1.1	−8.64	−7.06	−8.27
Lavangen	37	0.9	2.0	1.6	−8.16	−5.95	−7.34
Nordkjosbotn	76	0.9	2.5	1.8	−9.33	−5.55	−7.25
Storfjord	36	2.8	4.9	3.9	−4.46	0.22	−1.42
Ramfjord	49	0.5	2.9	1.6	−9.01	−6.47	−7.68
Kattfjord	59	0.1	1.1	0.3	−9.62	−6.9	−7.78

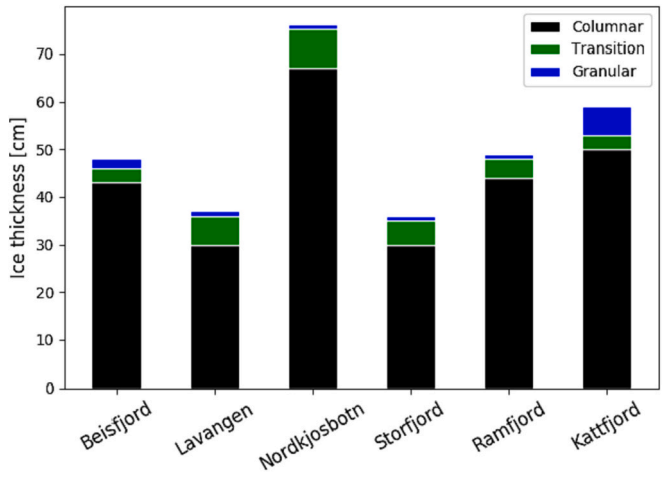

Fig. 3. Schematic of distribution of columnar (black), transition (green), and granular (blue) ice in the six ice cores gathered. (For interpretation of the references to colour in this figure legend, the reader is referred to the web version of this article.)

when temperatures increased above 0 °C.

Values for growth rate fall predominantly within the bounds given by Toyota et al. (2013) although some ice sections do exceed these limits when applying the model. Four cores have a calculated ice age within a week of the actual ice age, Beisfjord, Nordkjosbotn, Storfjord, and Ramfjord. The remaining two cores, Lavangen and Kattfjord, overestimate ice age substantially (Table 5).

4. Discussion

4.1. Implications of freshwater ice in fjord environment- influence on physical/biological properties

For five out of the six cores collected, the composition of water at the ice-ocean interface during ice growth ranged between 10 and 40% seawater equivalent to a salinity of 3 to 13 psu. This does not include all data from Kattfjord and Lavangen where results at certain depths ranged outside of bounds for growth rate (discussed further in Section 4.2). Hence, the ice gathered here was significantly influenced by freshwater runoff, which combined with minimal mixing, enabled a pronounced stable surface layer to form. When such a layer does form, with lower density than the ocean water beneath, convection confined to this layer can occur leading to efficient cooling (Farmer and Freeland, 1983). If the layer is <25 psu in salinity stratified cooling of the layer may occur (Weeks and Ackley, 1986).

The Baltic Sea offers another example of an Arctic region with low salinity ice, being generally <2 psu. In comparison to Norwegian fjords however, the Baltic is brackish with an ocean salinity between 1 and 9 psu (Granskog et al., 2006). Salinity of all ocean water sampled under the ice analyzed here was >30 psu. The large fraction of freshwater in all but the Storfjord core therefore reflects the presence of a distinct surface layer.

In Fig. 4, brine volume fraction is presented for all cores with values below 5% highlighted. This is an important range in the evolution of a sea ice as below this value, brine movement through the ice decreases, and hence the transport of heat, nutrients, and solute, preventing desalination (Polashenski et al., 2012; Arrigo et al., 1993; Golden et al., 1998). In cores collected from Lavangen and Storfjord, the brine volume fraction was >5% throughout. However, for all other cores, layers existed where brine volume fraction was below this value as well. This finding has several implications. From the ice surface downward, meltwater from snow and ice or wintertime rain (common in northern Norway) may not drain downward. This can alter the albedo of the ice as well as its signal at microwave and higher frequencies impacting how it is detected by remote sensing technology (Perovich, 1998; Tucker et al., 1992). In addition, the formation of melt ponds and decrease in albedo can accelerate melt, altering the length of time where ice is present in the fjord (Perovich et al., 2003; Polashenski et al., 2012). From the bottom of the ice upward, biota will not receive the nutrients needed to flourish (Arrigo et al., 2010; Kaartokallio et al., 2007). Lastly, the low permeability of certain layers if not the entire core will result in pollutants such as oil encapsulated in the ice, being unable to percolate upward, complicating clean-up methods (NORCOR, 1975; Oggier et al., 2019). Through analysis of the six ice samples here, clear differences are apparent between fjords that would impact the physical properties of sea ice. Therefore, attention should be placed on how much freshwater may be present at the ice-ocean interface of a fjord and its evolution through the winter season.

In Fig. 5, brine volume fraction is plotted as a function of F_{sw} derived assuming a constant growth rate of 1 cm/day ($1.16 \bullet 10^{-7}$ m s^{-1}), $S_{sw} = 32$, $\delta_{sw} = -0.5$ ‰ and $\delta_w = -11$ ‰. Curves for four different ice temperatures are presented. In Storfjord, the entirety of the ice volume had a value for F_{sw} above 0.5. At temperatures above −2 °C, the ice will stay well above 5% brine volume fraction, only decreasing below this value at temperatures closer to −5 °C. In Lavangen, F_{sw} ranged between 0.1

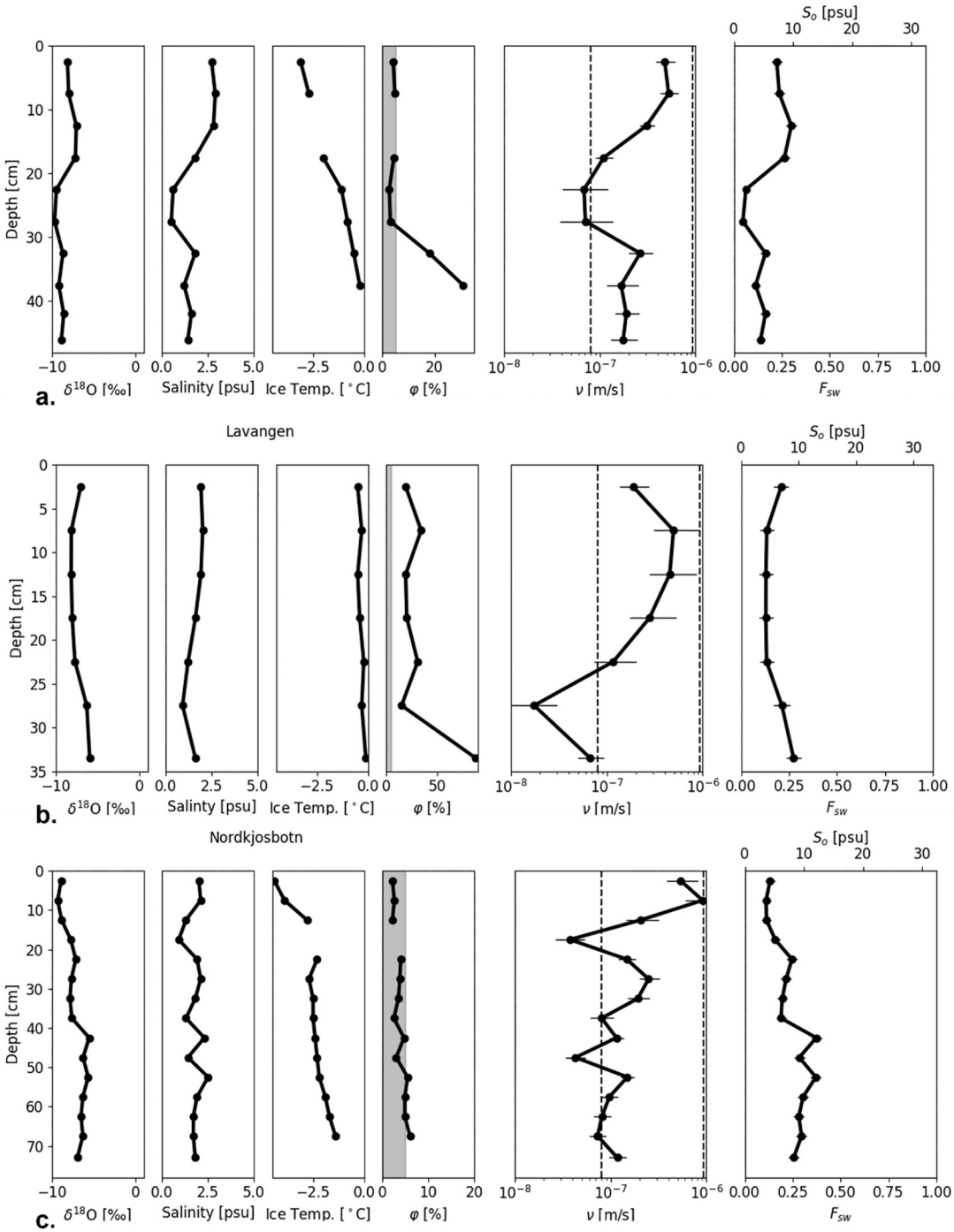

Fig. 4. From left to right- Measurements of bulk ice $\delta^{18}O$, salinity, temperature, calculated brine volume fraction (φ) and modelled results for growth rate (ν), and fraction of seawater at the ice – ocean interface (F_{sw}) for a) Beisfjord, b) Lavangen, and c) Nordkjosbotn. Shaded region marks BVF < 5%. From left to right- Measurements of bulk ice $\delta^{18}O$, salinity, temperature, calculated brine volume fraction (φ) and modelled results for growth rate (ν), and fraction of seawater at the ice – ocean interface (F_{sw}) for d) Storfjord, e) Ramfjord, and f) Kattfjord. Shaded region marks BVF < 5%.

and 0.3. With water at the ice-ocean interface composed of such a low fraction of seawater, ice must be above −1 °C to reach the higher brine volume fractions found (10–30%). With only slight decreases in temperature, ice that may have previously been permeable will become impermeable, introducing potentially complicated patterns of brine drainage as well as impacting the physical processes described above.

4.2. Systematic limitations of the method

Environmental conditions can only be derived by the model for periods where ice formation was significant compared to the thickness of the ice samples. In connection, it is blind to periods of air temperatures above the freezing point or periods with an ice–ocean interface heat flux that essentially prevented ice growth. The model applied to any ice sample will therefore be biased toward the interface conditions that existed during the fastest ice growth periods. Integrating the inverted

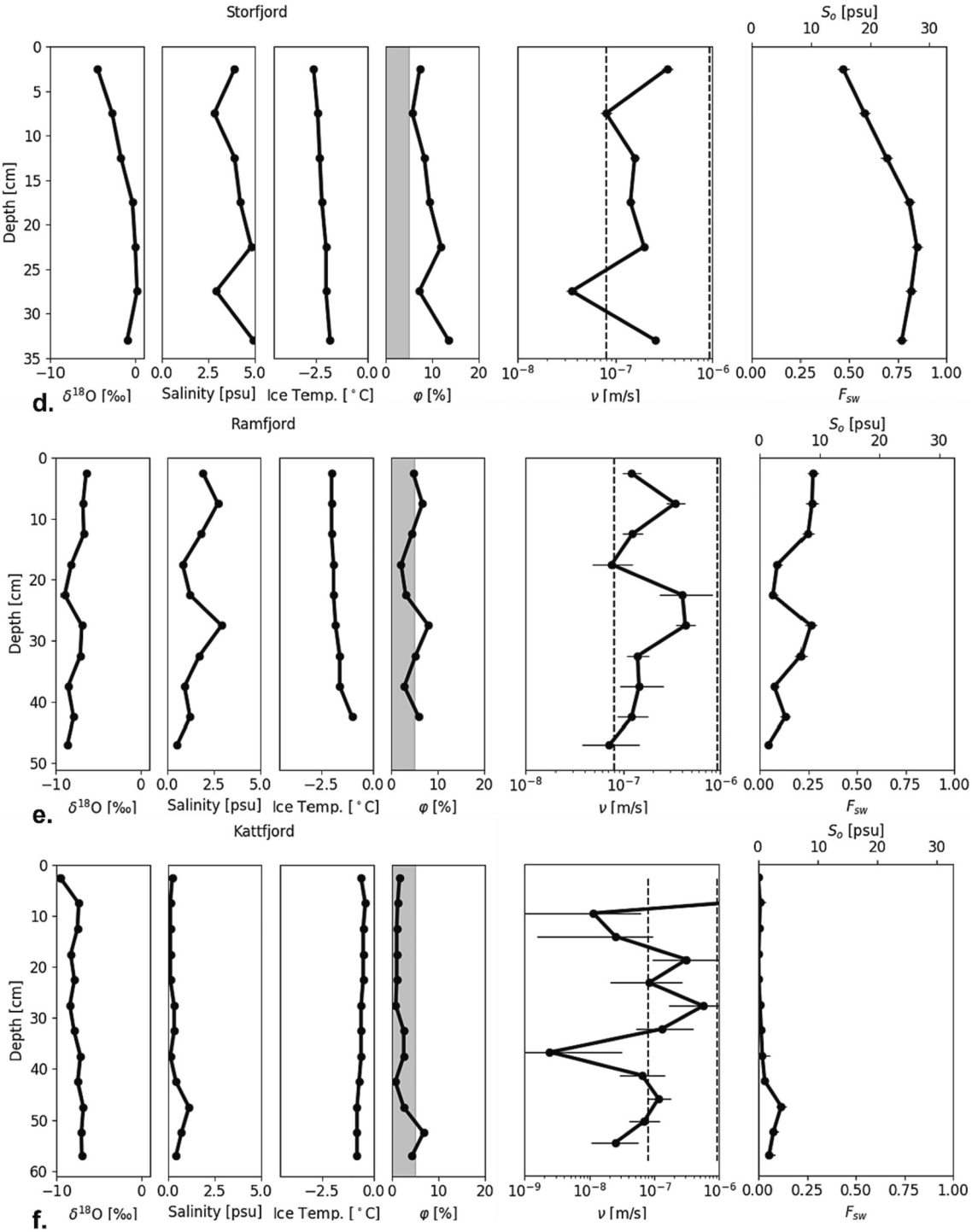

Fig. 4. (*continued*).

growth rate over the thickness of the ice should additionally provide a lower bound of the total ice age. However, if temperature deviations lead to episodic brine drainage and desalination (as described by Widell et al. (2006)), bulk ice salinity will decrease while $\delta^{18}O$ remains relatively constant, the latter's value being largely dependent on the ice rather than brine held in pores. This will result in the model producing unrealistically low growth rates in ice grown before the event and resultantly overestimations of ice age. The amount of ice impacted by brine drainage is currently not well characterized. Cores impacted by drainage may thus display sudden decreases in inverted growth rate.

Vastly overestimated ice ages are apparent in some cores of Table 5, indicating that episodic brine drainage may have altered physical properties of the ice significantly. The cores gathered at Kattfjord and Lavangen contain individual samples having unrealistically low growth rates, as displayed in Fig. 4f and Fig. 4b, respectively. In Fig. 6, air temperature in Kattfjord is shown to reach above freezing on several occasions with a minimum air temperature of −10.5 °C, maximum air temperature of 4 °C, and average air temperature of −5.3 °C being higher than at all other fjords (Table 4). For this reason, it is likely periods of little growth or possibly melt occurred accompanied by brine drainage. In Lavangen, one day of above freezing temperatures is apparent, reaching only up to 0.5 °C, making the cause of brine drainage

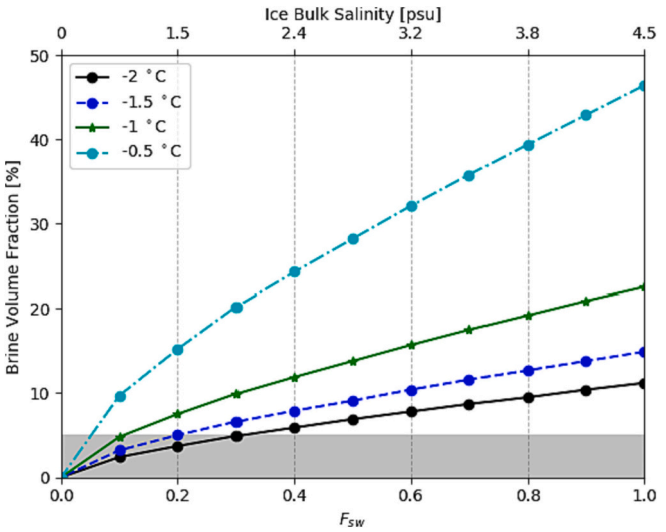

Fig. 5. Brine volume fraction as a function of the fraction of seawater at the ice – ocean interface and corresponding ice bulk salinity for ice with growth rate $\nu = 1.16 \bullet 10^{-7}$ m s^{-1} for four temperatures between −2 and 0 °C.

less clear. The result from Lavangen, however, highlights the importance of considering heat flux through the ice due to both ocean and air temperature. Ocean temperature in Lavangen, was generally warmer than all but Beisfjord, being above 2 °C throughout the period with ice and increasing to over 4 °C on several days. Oceanic heat flux, a function of both water temperature and current, likely influenced growth in all fjords. In Lavangen, however, its influence is exemplified in potentially altering heat flux through the ice, resulting in warming and possibly brine drainage.

For both Storfjord and Beisfjord, air temperatures remained relatively low as most of the ice growth occurred. Despite average and minimum air temperatures being the lowest (Storfjord) and third lowest (Beisfjord) (Table 4), growth rate was relatively slow throughout much of each core in comparison to other fjords (Fig. 4). Beisfjord showed a clear decrease in growth rate, going slightly below the limits set forth by Toyota et al. (2013) but with no abrupt jumps indicative of brine drainage. At Storfjord, one abrupt decrease is evident between 25 and 30 cm, likely the result of brine drainage due to the increase in temperature experienced on 2 March 2018. The impact of ocean heat must again be considered in addition to air temperature. As opposed to causing brine drainage or melt, however, heat flux is hypothesized to have remained high enough through the ice due to low air temperatures to allow for consistent, slow growth. This is an example of how results of the model supplemented by weather and ocean data, can offer a glimpse into fjord and ice conditions and the interplay of air, ocean, and ice despite a lack of in situ measurements.

With an increase in temperature to above 0 °C, melt of the ice and snow at the surface as well as rain are all possible and can occur throughout winter in the six fjords considered here. Therefore, in addition to brine drainage, the drainage of ice melt, snowmelt, and rain must also be considered. When this occurs, ice salinity will further decrease and ice temperature will increase as heat is transported with the melt (Notz and Worster, 2009). Similar to brine drainage, the impact will be greatest on bulk ice salinity but low values of $\delta^{18}O$ for rain and snowmelt may also act to lower the bulk ice value of this property.

Differences in δ_w are apparent in Table 2, being the result of the different geographical location of rivers leading into each fjord. When calculations are adapted to incorporate a range in values for δ_w as well as $\delta_{sw,}$ and S_{sw}, the impact is strongest on growth rate as opposed to the fraction of seawater present at the interface. Investigating these results further reveals that for the samples where the fraction of seawater is lowest, and thus fraction of freshwater highest, growth rate calculations are most sensitive to variations in δ_w. For ice samples not suspected of being influenced by brine drainage, a small variation in δ_w can cause a noticeable shift in growth rate. This is displayed in Table 5 where estimates of ice age move closer to actual ice age when uncertainties in endmembers are considered. Ideally, a sample of δ_w would therefore be obtained on the day of ice formation as opposed to only a sample on the day of coring to provide the most accurate results. For Storfjord, where F_{sw} was highest, the influence of uncertainties on model results is minimal. The reason is related to the smaller fluctuation observed in δ_{sw} in comparison to δ_w (0.3 ‰ versus 0.4 ‰). Being formed from water having a higher fraction of seawater, the Storfjord core was thus more sensitive to variations in δ_{sw} and therefore displays a smaller range in values.

5. Summary and conclusions

During March 2018, ice cores were collected at six fjords located in northern Norway to obtain measurements of bulk ice salinity, temperature, and $\delta^{18}O$. Salinity and the isotopic signature of ice depend on growth rate and conditions at the ice-ocean interface making interpretation of profiles non-trivial. Using relationships from the literature, a method was developed to invert bulk ice salinity and $\delta^{18}O$ simultaneously to determine the history of growth rate and interface composition. Quantitative results depend on knowledge of salinity and $\delta^{18}O$ of both freshwater leading into the fjord and seawater and can reveal notable periods of change in the growth history.

It was found that five of the six investigated sites had ice grown from a brackish layer with between 0 and 40% seawater content, while one site had ice grown from water with between 50 and 90% seawater content highlighting the strong influence of freshwater input on ice growth and conditions in a fjord. The brine volume fraction of ice was found to be largely below 5% for four out of the six fjords. With sea ice bulk salinities as low as those observed in this study, even at temperatures above −2 °C ice may continue to have a brine volume fraction lower than this value. The substantial influence of freshwater on ice growth should also be considered when estimating other physical and biological properties of fjord ice.

While the method used here proved valuable to obtain a general estimation of freshwater influence on ice growth in a fjord, limitations must be considered with this study also supporting the following findings:

- Substantial periods of air temperatures approaching the melting point of ice will bias the model toward either slow or fast growth rates. Such periods of warm weather may modify ice properties due to brine drainage, meltwater/rain drainage, and changes at the interface water due to snow or ice melt and isotopic composition of the freshwater source.
- Estimates of ice age determined from results for growth rate had an accuracy of less than one week for four fjords. The bulk of the error in the remaining fjords can be attributed to individual samples that were expected to have grown under unrealistically low growth rates. However, periods where temperature was near to 0 °C occurred at almost all sites, indicating that errors in the aggregate ice age are to be expected.
- The quality of the model depends on the accuracy to which the endmembers are known. Sensitivity is highest to uncertainties in the properties of the dominating water mass, i.e. applying the model to ice of predominantly seawater origin will be most sensitive to knowledge of seawater properties. In the current study, sensitivity was highest to uncertainties in the isotopic composition of the river water, δ_w. In Norwegian fjords, the dominating water mass of ice of a fjord may differ between seasons (O'Sadnick et al., 2022).

CRediT authorship contribution statement

Megan O'Sadnick: Conceptualization, Methodology, Software,

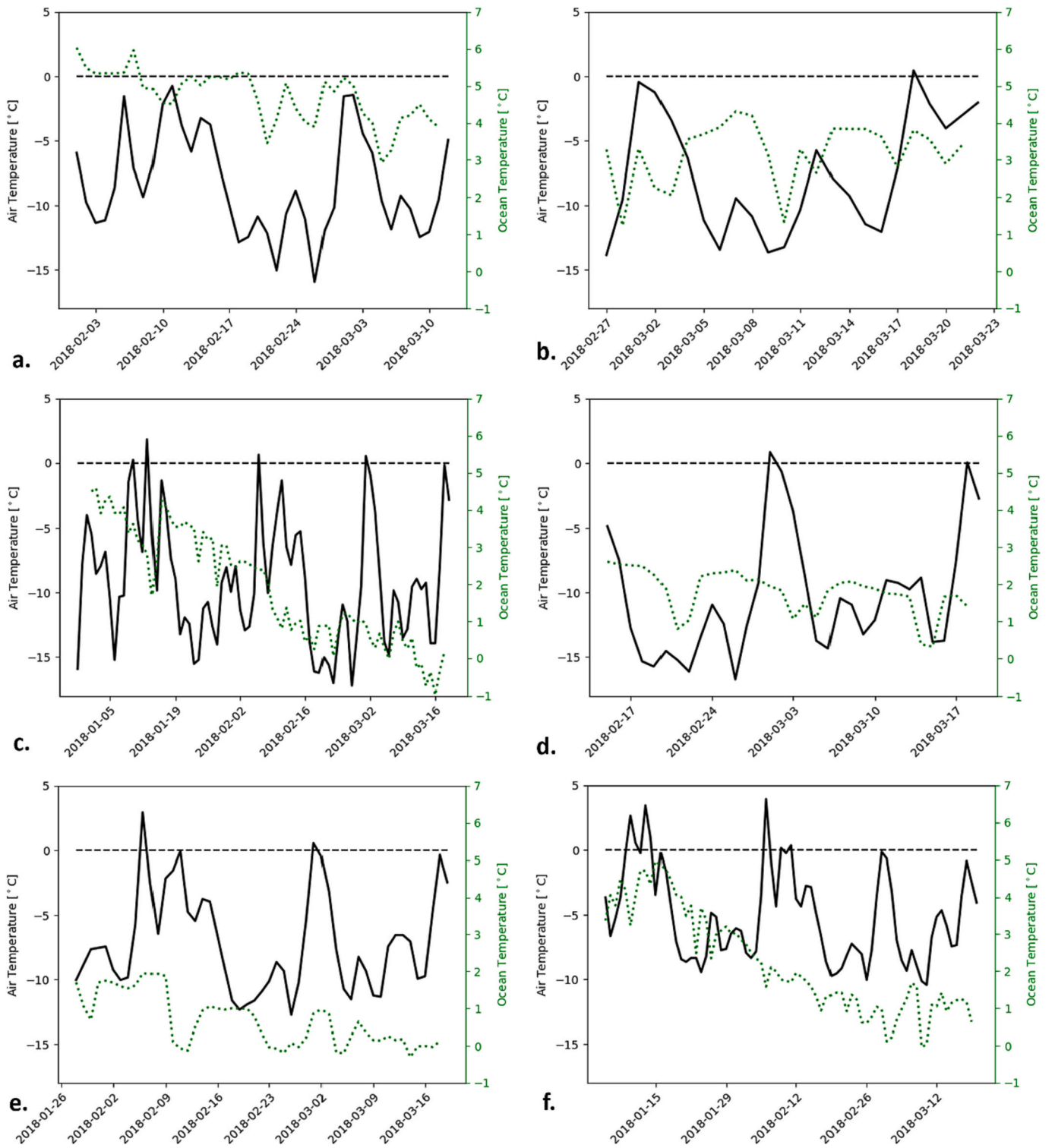

Fig. 6. Air temperature and ocean surface temperature from the time of ice formation until measurement for a) Beisfjord, b) Lavangen, c) Nordkjosbotn, d) Storfjord, e) Ramfjord, f) Kattfjord.

Validation, Formal analysis, Investigation, Data curation, Writing – original draft, Writing – review & editing, Visualization. **Chris Petrich:** Conceptualization, Methodology, Software, Resources, Writing – review & editing, Supervision, Project administration, Funding acquisition. **Jofrid Skarðhamar:** Resources, Writing – review & editing, Supervision.

Declaration of Competing Interest

The authors declare that they have no known competing financial interests or personal relationships that could have appeared to influence the work reported in this paper.

Table 4
Summary of air temperatures obtained through SeNorge.

Fjord	T_{avg} [°C]	T_{min} [°C]	T_{max} [°C]	Days above freezing	θ [° days]
Beisfjord	−8.3	−16.0	−0.8	0	334
Lavangen	−7.6	−13.9	0.5	1	182
Nordkjosbotn	−9.3	−17.3	1.2	4	750
Storfjord	−10.3	−16.8	0.9	2	340
Ramfjord	−7.2	−12.8	3.0	2	367
Kattfjord	−5.3	−10.5	4.0	7	394

Table 5
Comparison of actual ice age on day of measurement derived using satellite imagery, the estimated ice age calculated using results from the model, and the range in ice age possible considering uncertainties in endmembers.

	Age of Ice (days)		
Fjord	Actual	Calculated	Range
Beisfjord	40	37	24–55
Lavangen	24	58	36–93
Nordkjosbotn	81	86	67–109
Storfjord	34	39	34–43
Ramfjord	51	41	27–60
Kattfjord	75	364	60–4.0•10^{14}

Data availability

Measurements of ice bulk salinity and δ18O, seawater salinity and δ18O, and freshwater δ18O can be accessed at https://doi.org/10.5281/zenodo.6607169. All other data available at request.

Acknowledgements

This work was funded by the Centre for Integrated Remote Sensing and Forecasting for Arctic Operations (CIRFA), a Centre for Research-based Innovation (Research Council of Norway project number 237906), and partners. Comments from Jean-Luis Tison, Pat Langhorne, and Mats Granskog on an early draft are gratefully acknowledged as well as comments from an anonymous reviewer in a subsequent version.

References

Alkire, M.B., Nilsen, F., Falck, E., Søreide, J., Gabrielsen, T.M., 2015. Tracing sources of freshwater contributions to first-year sea ice in Svalbard fjordss. Cont. Shelf Res. 101, 85–97. https://doi.org/10.1016/j.csr.2015.04.003.

Arrigo, K., Kremer, J., Sullivan, C., 1993. A simulated Antarctic ast ice ecosystem. J. Geophys. Res. Ocean. 98, 6929–6946. https://doi.org/10.1029/93JC00141.

Arrigo, K., Mock, T., Lizotte, M., 2010. Primary producers and sea ice. In: Thomas, D., Dieckmann, G. (Eds.), Sea Ice. Wiley-Blackwell, Oxford, pp. 283–326.

Asplin, L., Salvanes, A.G.V., Kristoffersen, J.B., 1999. Nonlocal wind-driven fjord–coast advection and its potential effect on plankton and fish recruitment. Fish. Oceanogr. 8 (4), 255–263.

Aure, J., Molvær, J., Stigebrandt, A., 1996. Observations of inshore water exchange forced by a fluctuating offshore density field. Marine Pollut. Bull. 33 (1–6), 112–119.

Burton, J.A., Prim, R.C., Slichter, W., 1953. P.: the distribution of solute in crystals grown from the melt. Part I. Theoretical. J. Chem. Phys. 21, 1987–1991. https://doi.org/10.1063/1.1698728.

Copernicus Sentintel Data, 2019. Retrieved from Google Earth Engine, processed by the European Space Agency.

Cottier, F.R., Nilsen, F., Skogseth, R., Tverberg, V., Skarðhamar, J., Svendsen, H., 2010. Arctic fjords: a review of the oceanographic environment and dominant physical processes. Geol. Soc. London Spec. Publ. 344, 35–50. https://doi.org/10.1144/SP344.4.

Cox, G.F.N., Weeks, W.F., 1975. Brine Drainage and Initial Salt Entrapment in Sodium Chloride Ice. US Army Corps Eng Cold Reg Res Eng Lab Res Rep.

Cox, G.F., Weeks, W.F., 1983. Equations for determining the gas and brine volumes in sea - ice samples. J. Glaciol. 29, 306–316.

Craig, H., Hom, B., 1968. Relationships of deuterium, oxygen 18, and chlorinity in the formation of sea ice. Trans. AGU 49, 216–217.

Dalsøren, S.B., Albretsen, J., Asplin, L., 2020. New validation method for hydrodynamic fjord models applied in the Hardangerfjord, Norway. Estuar. Coast. Shelf Sci. 246 https://doi.org/10.1016/j.ecss.2020.107028.

Eicken, H., 1998. Deriving modes and rates of ice growth in the weddell sea from microstructural, salinity and stable-isotope data. Antarct. Sea Ice Phys. Process. Interact. Var Antarct. Res. Ser 74, 89–122. https://doi.org/10.1029/ar074p0089.

Farmer, D.M., Freeland, H.J., 1983. The physical oceanography of Fjords. Prog. Oceanogr. 12, 147–220. https://doi.org/10.1016/0079-6611(83)90004-6.

Golden, K.M., Ackley, S.F., Lytle, V.I., 1998. The percolation phase transition in sea ice. Science (80-.) 282, 2238–2241.

Granskog, M., Kaartokallio, H., Kuosa, H., Thomas, D.N., Vainio, J., 2006. Sea ice in the Baltic Sea - a review. Estuar. Coast. Shelf Sci. 70, 145–160. https://doi.org/10.1016/j.ecss.2006.06.001.

Green, J.A.M., Molvaer, J., Stigebrandt, A., 2004. Hydrographic response of Holandsfjord to changed freshwater runoff. J. Geophys. Res. C Ocean. 109, 1–10. https://doi.org/10.1029/2004JC002295.

Hunke, E.C., Notz, D., Turner, A.K., Vancoppenolle, M., 2011. The Multiphase Physics of Sea Ice: A Review for Model Developers, 5, pp. 989–1009. https://doi.org/10.5194/tc-5-989-2011.

Inall, M.E., Gillibrand, P.A., 2010. The physics of mid-latitude fjords: a review. Geol. Soc. Spec. Publ. 344, 17–33. https://doi.org/10.1144/SP344.3.

Kaartokallio, H., Kuosa, H., Thomas, D.N., Granskog, M.A., Kivi, K., 2007. Biomass, composition and activity of organism assemblages along a salinity gradient in sea ice subjected to river discharge in the Baltic Sea. Polar Biol. 30, 183–197. https://doi.org/10.1007/s00300-006-0172-z.

Kujawa, A., Łącka, M., Szymańska, N., Pawłowska, J., Telesiński, M.M., Zajączkowski, M., 2021. Could Norwegian fjords serve as an analogue for the future of the Svalbard fjords? State and fate of high latitude fjords in the face of progressive "atlantification,". Polar Biol. 44, 2217–2233. https://doi.org/10.1007/s00300-021-02951-z.

LeGrande, A.N., Schmidt, G.A., 2006. Global gridded data set of the oxygen isotopic composition in seawater. Geophys. Res. Lett. 33 (12).

Lehmann, M., Siegenthaler, U., 1991. Equilibrium oxygen- and hydrogen-isotope fractionation between ice and water. J. Glaciol. 37, 23–26. https://doi.org/10.1017/s0022143000042751.

Leppäranta, M., Manninen, T., 1988. The Brine and Gas Content of Sea Ice with Attention to Low Salinities and High Temperatures, Helsinki, 14 pp.

Lussana, C., Saloranta, T., Skaugen, T., Magnusson, J., Einar Tveito, O., Andersen, J., 2018. SeNorge2 daily precipitation, an observational gridded dataset over Norway from 1957 to the present day. Earth Syst. Sci. Data 10, 235–249. https://doi.org/10.5194/essd-10-235-2018.

Macdonald, R.W., Paton, D.W., Carmack, E.C., 1995. The freshwater budget and under-ice spreading of Mackenzie River water in the Canadian Beaufort Sea based on salinity and 18O/16O measurements in water and ice. J. Geophys. Res. 100, 895–919.

Macdonald, R.W., Carmack, E.C., Paton, D.W., 1999. Using the d 18 O composition in landfast ice as a record of arctic estuarine processes. Mar. Chem. 65, 3–24.

Melling, H., Moore, R., 1995. Modification of halocline source waters during freezing on the Beaufort Sea shelf: evidence from oxygen isotopes and dissolved nutrients. Cont. Shelf Res. 15, 89–113.

Nakawo, M., Sinha, N.K., 1981. Growth rate and salinity profile of first-year sea ice in the High Arctic. J. Glaciol. 27, 313–328. https://doi.org/10.1017/s0022143000015409.

Nan, Y., Tian, F., Hu, H., Wang, L., Zhao, S., 2019. Stable isotope composition of river waters across the world. Water 11 (9), 1760.

NORCOR, 1975. The Interaction of Crude Oil with Arctic Sea Ice, Beaufort Sea Technical Report, Victoria, BC, Canada.

Notz, D., Worster, M.G., 2009. Desalination processes of sea ice revisited. J. Geophys. Res. Ocean. 114, 1–10. https://doi.org/10.1029/2008JC004885.

Oggier, M., Eicken, H., Petrich, C., Wilkinson, J., O'Sadnick, M., 2019. Crude oil migration in sea-ice: Laboratory studies of constraints on oil mobilization and seasonal evolution. Cold Reg. Sci. Technol. 102924.

Olsen, J., Carter, N.A., Dawson, J., 2019. Community perspectives on the environmental impacts of Arctic shipping: case studies from Russia, Norway and Canada. Cogent Soc. Sci. 5 https://doi.org/10.1080/23311886.2019.1609189.

O'Sadnick, M., 2022. Ice Core Measurements - Northern Norwegian Fjord Ice - Winter 2018/2019 (1.0.0) [Data set]. https://doi.org/10.5281/zenodo.6607169.

O'Sadnick, M., Petrich, C., Brekke, C., Skarðhamar, J., 2020. Ice extent in sub-arctic fjords and coastal areas from 2001 to 2019 analyzed from MODIS imagery. Ann. Glaciol. https://doi.org/10.1017/aog.2020.34.

O'Sadnick, M., Petrich, C., Brekke, C., Skarðhamar, J., Kleven, Ø., 2022. Ice conditions in northern Norwegian fjords: Observations and measurements from three winter seasons, 2017–2020. Cold Reg. Sci. Technol. 103663 https://doi.org/10.1016/j.coldregions.2022.103663.

Perovich, D., 1998. Optical properties of sea ice. In: Leppäranta, M. (Ed.), Physics of Ice-Covered Seas. University of Helsinki, Helsinki, pp. 195–230.

Perovich, D.K., Grenfell, T.C., Richter-Menge, J.A., Light, B., Tucker, W.B., Eicken, H., 2003. Thin and thinner: Sea ice mass balance measurements during SHEBA. J. Geophys. Res. Ocean. 108, 1–21. https://doi.org/10.1029/2001jc001079.

Petrich, C., Langhorne, P., Eicken, H., 2011. Modelled bulk salinity of growing first-year. In: Proc. 21st Int. Conf. Port Ocean Eng. under Arct. Cond.

Polashenski, C., Perovich, D., Courville, Z., 2012. The mechanisms of sea ice melt pond formation and evolution. J. Geophys. Res. Ocean. 117, 1–23. https://doi.org/10.1029/2011JC007231.

Skreslet, S., Loeng, H., 1977. Deep water renewal and associated processes in Skjomen, a fjord in North Norway. Estuar. Coast. Mar. Sci. 5, 383–398. https://doi.org/10.1016/0302-3524(77)90063-9.

Smith, I.J., Langhorne, P.J., Frew, R.D., Vennell, R., Haskell, T.G., 2012. Sea ice growth rates near ice shelves. Cold Reg. Sci. Technol. 83–84, 57–70. https://doi.org/10.1016/j.coldregions.2012.06.005.

Souchez, R., Tison, J.-L., 1987. Freezing rate determination by the isotopic composition of the ice. Geophys. Res. Lett. 14, 599–602.
Souchez, R., Tison, J.-L., 1988. Deuterium concentration and growth rate of antarctic first-year sea ice. Geophys. Res. Lett. 15, 1385–1388.
Stigebrandt, A., 2012. In: Bengtsson, L., Herschy, R.W., Fairbridge, R.W. (Eds.), Hydrodynamics and Circulation of Fjords, in: Encyclopedia of Lakes and Reservoirs. Encyclopedia of Earth Sciences Series. Springer, Dordrecht. https://doi.org/10.5860/choice.50-3613.
Svavarsson, J., Guls, H.D., Sham, R.C., Leung, K.M.Y., Halldórsson, H.P., 2021. Pollutants from shipping - new environmental challenges in the subarctic and the Arctic Ocean. Mar. Pollut. Bull. 164 https://doi.org/10.1016/j.marpolbul.2021.112004.
Toyota, T., Smith, I.J., Gough, A.J., Langhorne, P.J., Leonard, G.H., Van Hale, R.J., Mahoney, A.R., Haskell, T.G., 2013. Oxygen isotope fractionation during the freezing of sea water. J. Glaciol. 59, 697–710. https://doi.org/10.3189/2013JoG12J163.
Tucker, W.B., Perovich, D.K., Gow, A.J., Weeks, W.F., Drinkwater, M., 1992. R.: Physical properties of sea ice relevant to remote sensing. Microw. Remote Sens. Sea Ice 68, 9–28.
Vonnahme, T., 2020. R.: Microbial Diversity and Ecology in the Coastal Arctic Seasonal Ice Zone. UiT The Arctic University of Norway, pp. 1–238.
Wassmann, P., Svendsen, H., Keck, a., and Reigstad, M., 1996. Selected aspects of the physical oceanography and particle fluxes in fjords of northern Norway. J. Mar. Syst. 8, 53–71. https://doi.org/10.1016/0924-7963(95)00037-2.
Weeks, W.F., Ackley, S.F., 1986. The growth, structure, and properties of sea ice. In: Untersteiner, N. (Ed.), The Geophysics of Sea Ice. Plenum Press, New York, pp. 9–164.
Weeks, W.F., Lofgren, G., 1967. The effective solute distribution coefficient during the freezing of NaCl solutions. University, Hokkaido, pp. 579–597.
Widell, K., Fer, I., Haugan, P.M., 2006. Salt release from warming sea ice. Geophys. Res. Lett. 33, 1–5. https://doi.org/10.1029/2006GL026262.
Worster, M.G., 1997. Convection in Mushy Layers. Annu. Rev. Fluid Mech. 29, 91–122. https://doi.org/10.1146/annurev.fluid.29.1.91.